Acta Biomaterialia 113 (2020) 130–143

Contents lists available at ScienceDirect

Acta Biomaterialia

journal homepage: www.elsevier.com/locate/actbio

Full length article

3D printing of fibre-reinforced cartilaginous templates for the regeneration of osteochondral defects

Susan Critchley[a,b,1], Eamon J. Sheehy[a,c,d,1], Gráinne Cunniffe[a,b], Pedro Diaz-Payno[a,b], Simon F. Carroll[a,b], Oju Jeon[e], Eben Alsberg[e,f], Pieter A.J. Brama[g], Daniel J. Kelly[a,b,c,d,*]

[a] Trinity Centre for Biomedical Engineering, Trinity Biomedical Sciences Institute, Trinity College Dublin, Dublin, Ireland
[b] Department of Mechanical and Manufacturing Engineering, School of Engineering, Trinity College Dublin, Dublin, Ireland
[c] Advanced Materials and Bioengineering Research Centre, Trinity College Dublin and Royal College of Surgeons in Ireland, Dublin, Ireland
[d] Tissue Engineering Research Group, Department of Anatomy and Regenerative Medicine, Royal College of Surgeons in Ireland, Dublin, Ireland
[e] Department of Bioengineering, University of Illinois, Chicago, IL, USA
[f] Departments of Orthopaedics, Pharmacology, and Mechanical & Industrial Engineering, University of Illinois, Chicago, IL, USA
[g] School of Veterinary Medicine, University College Dublin, Dublin, Ireland

ARTICLE INFO

Article history:
Received 31 March 2020
Revised 27 May 2020
Accepted 28 May 2020
Available online 4 June 2020

Keywords:
3D Printing
Biofabrication
Mesenchymal stem cell
Endochondral
Chondrogenesis
Osteochondral

ABSTRACT

Successful osteochondral defect repair requires regenerating the subchondral bone whilst simultaneously promoting the development of an overlying layer of articular cartilage that is resistant to vascularization and endochondral ossification. During skeletal development articular cartilage also functions as a surface growth plate, which postnatally is replaced by a more spatially complex bone-cartilage interface. Motivated by this developmental process, the hypothesis of this study is that bi-phasic, fibre-reinforced cartilaginous templates can regenerate both the articular cartilage and subchondral bone within osteochondral defects created in caprine joints. To engineer mechanically competent implants, we first compared a range of 3D printed fibre networks (PCL, PLA and PLGA) for their capacity to mechanically reinforce alginate hydrogels whilst simultaneously supporting mesenchymal stem cell (MSC) chondrogenesis *in vitro*. These mechanically reinforced, MSC-laden alginate hydrogels were then used to engineer the endochondral bone forming phase of bi-phasic osteochondral constructs, with the overlying chondral phase consisting of cartilage tissue engineered using a co-culture of infrapatellar fat pad derived stem/stromal cells (FPSCs) and chondrocytes. Following chondrogenic priming and subcutaneous implantation in nude mice, these bi-phasic cartilaginous constructs were found to support the development of vascularised endochondral bone overlaid by phenotypically stable cartilage. These fibre-reinforced, bi-phasic cartilaginous templates were then evaluated in clinically relevant, large animal (caprine) model of osteochondral defect repair. Although the quality of repair was variable from animal-to-animal, in general more hyaline-like cartilage repair was observed after 6 months in animals treated with bi-phasic constructs compared to animals treated with commercial control scaffolds. This variability in the quality of repair points to the need for further improvements in the design of 3D bioprinted implants for joint regeneration.

Statement of Significance

Successful osteochondral defect repair requires regenerating the subchondral bone whilst simultaneously promoting the development of an overlying layer of articular cartilage. In this study, we hypothesised that bi-phasic, fibre-reinforced cartilaginous templates could be leveraged to regenerate both the articular cartilage and subchondral bone within osteochondral defects. To this end we used 3D printed fibre networks to mechanically reinforce engineered transient cartilage, which also contained an overlying layer of phe-

* Corresponding author: Trinity Centre for Biomedical Engineering, Trinity Biomedical Sciences Institute, Trinity College Dublin, Dublin, Ireland.
E-mail address: kellyd9@tcd.ie (D.J. Kelly).
[1] Both the authors contributed equally to this work.

https://doi.org/10.1016/j.actbio.2020.05.040

notypically stable cartilage engineered using a co-culture of chondrocytes and stem cells. When chondrogenically primed and implanted into caprine osteochondral defects, these fibre-reinforced bi-phasic cartilaginous grafts were shown to spatially direct tissue development during joint repair. Such developmentally inspired tissue engineering strategies, enabled by advances in biofabrication and 3D printing, could form the basis of new classes of regenerative implants in orthopaedic medicine.

1. Introduction

Treating osteochondral (OC) defects requires supporting subchondral bone repair whilst simultaneously regenerating articular cartilage that is resistant to vascularisation and endochondral ossification. Common approaches to the tissue engineering of articular cartilage and bone involve the encapsulation of cells and/or growth factors into scaffolds or hydrogels [1–12], or the use of scaffold-free or self-assembly approaches, particularly for articular cartilage engineering [3],[13–17]. Combining different approaches for cartilage and bone repair into multi-layered constructs has also formed the basis of different osteochondral tissue engineering strategies [4,18,19], although successfully regenerating the osteochondral interface remains a significant challenge. In recent years there has been increased interest in recapitulating developmental processes as a means of promoting regeneration of the adult skeleton [20–24]. Motivated by the fact that the articular layer of synovial joints also functions as a surface growth plate during postnatal development [25], with a cartilaginous precursor preceding the osteochondral unit, we have previously engineered osteochondral tissues by spatially regulating endochondral ossification within engineered cartilage templates [19]. The 'chondral' region of these engineered tissues consisted of a co-culture of mesenchymal stem cells (MSCs) and chondrocytes, which we and others have shown can promote the development of a cartilage tissue resistant to hypertrophy and mineralisation [19,26–28], while the osseous region was generated using bone marrow MSC-laden hydrogels primed for chondrogenesis and endochondral ossification. However, this proof-of-principle study was performed in a subcutaneous environment and, consequently, the engineered constructs were not subjected to the high levels of mechanical load they will experience upon implantation into a damaged or diseased joint. Therefore, new biofabrication strategies are required to develop mechanically reinforced hydrogels that not only have bulk mechanical properties compatible with implantation into load bearing defects, but which also provides a cellular environment compatible with differentiation and matrix synthesis.

Strategies to enhance the mechanical properties of hydrogels include increasing the concentration of the bulk material [10,29], the degree or type of cross-linking [30–33] and the creation of interpenetrating polymer networks (IPNs) [34,35]. Increasing hydrogel concentration and/or cross-linking density to increase implant stiffness can have a negative impact on cellular activity, degradation kinetics, permeability, the diffusion of nutrients and waste removal [10,36–38]. Furthermore, the hydrogel itself can become a barrier to extracellular matrix (ECM) development [39,40]. Moreover, such changes can impact the differentiation of encapsulated stem cells, with stiffer hydrogels more conducive to osteogenesis or an endochondral phenotype, which is undesirable in the context of articular cartilage tissue engineering [41–43]. In recent years, multiple tool biofabrication has been used to engineer composite constructs consisting of cell-laden hydrogels mechanically reinforced with polymer networks [44–47]. For example, reinforcing gelatine methacrylate (gelMA) hydrogels with melt-electrowritten polycaprolactone (PCL) fibres (<100 μm diameter) resulted in the development of constructs with mechanical properties superior to that of the hydrogel or scaffold alone, which could be tailored further to mimic the mechanical properties of articular cartilage [48]. The advantage of such approaches is that the hydrogel phase can be engineered to provide a stiffness and composition compatible with supporting a specific cellular phenotype, and can be decoupled from the reinforcing polymer phase, which provides the bulk strength and stiffness to the composite implant.

Identifying a suitable reinforcing polymer network material will be integral to the success of such composite engineered tissues. PCL is a widely used polymer for 3D printing due to its low printing temperature (59–64 °Celsius) [49], biocompatibility and mechanical properties [50]. The mechanical properties can be tailored by modulating the molecular weight, strand size, printed architecture and strand spacing [51,52]. However, PCL has a long degradation time (approximately 2–3 years [53]), during which matrix deposition could be inhibited by the persistence of material at the site of injury. Poly(lactic acid) (PLA) and poly(lactic-co-glycolic acid) (PLGA) are also widely used in the medical field, as both are biocompatible, with good mechanical properties, with PLGA having a much faster degradation rate than PCL [54–56]. They have been used for drug/ growth factor delivery, as porous scaffolds [49,57–59] and can be 3D printed [60]. One drawback of PLA/PLGA materials, however, is that their melting temperatures are much higher than PCL (~130 °Celsius for PLGA and ~180 °Celsius for PLA), which can render the co-printing of live cells with PLA/PLGA a challenge. The degradation of PLGA is defined by the ratio of lactic acid to glycolic acid, with PLGA 50:50 having a degradation time of 1–2 months and 85:15 5–6 months [49]. A significant concern is the release of acids as degradation products that can induce inflammation [61–63]. The suitability of different 3D printed polymer networks (PCL, PLA and PLGA) for mechanically reinforcing engineered tissues for cartilage, bone and osteochondral defect repair has yet to be appropriately assessed.

The hypothesis of this study is that fibre reinforced engineered cartilage templates are capable of promoting the regeneration of critically sized osteochondral defects in a translational large animal model, supporting stable hyaline cartilage development at the articular surface and endochondral bone development in the underlying subchondral region of the implant. To fabricate mechanically functional implants, 3D printing was first used to create networks of PLA, PLGA (65:35 and 85:15) and PCL fibers to mechanically reinforce MSC-laden hydrogels. The mechanical properties and swelling characteristics of these constructs were first assessed, as was their capacity to support chondrogenesis of MSCs *in vitro*. Based on this analysis, appropriately reinforced MSC-laden alginate hydrogels were then utilised as the osseous (also termed endochondral) layer of bi-phasic constructs, with the overlying articular cartilage phase consisting of a stem cell-chondrocyte co-culture, engineered either by self-assembly (SA), or by cellular encapsulation within alginate or agarose hydrogels. Thereafter, the capacity of these chondrogenically primed bi-phasic constructs to support the development of a vascularised bone-like tissue overlaid by a phenotypically stable layer of hyaline cartilage was assessed fol-

Table 1
Printing parameters for reinforcing polymers.

Material	Molecular weight	Tank temp °C	Needle temp °C	Pressure MPa	Screw speed
PCL	48–90,000	70	70	0.1	9 rev/m
PLA	60,000	180	160	0.1	20 rev/m
PLGA 85:15	50–75,000	145	130	0.1	20 rev/m
PLGA 65:35	40–75,000	140	120	0.1	16 rev/m

lowing subcutaneous implantation into nude mice. Finally, the capacity of these bi-phasic cartilage templates to promote the regeneration of critically sized osteochondral defects was assessed in a pre-clinical, large animal (goat) model .

2. Material and methods

2.1. 3D printing process

A 3D bioprinter was used for printing of polymers (RegenHU, Switzerland). The orthogonal architecture (6 mm diameter, 4–6 mm height, 1.5 mm line spacing) was designed on the accompanying software, BioCAD. PCL, PLA, PLGA 85:15, PLGA 65:35 (all Sigma-Aldrich) were heated in the extruding tank at temperatures and extruded through a 25-gauge needle (individual parameters are shown in Table 1). All reinforcement cages were then sterilised with ethylene oxide (EtO) for 12 h (Anprolene, Andersen Products, USA). Thereafter, they were subjected to aeration in a laminar flow hood for 24 h to ensure dissipation of the ethylene oxide gas.

2.2. Cell isolation and expansion

Bone marrow derived stem cells (BMSCs), chondrocytes and fat pad derived stem cells (FPSCs) were obtained from either porcine or goat donors and were expanded in high-glucose Dulbecco's Modified Eagle Medium (hgDMEM) (GlutaMAX™; Biosciences, Ireland) supplemented with 10% foetal bovine serum (FBS), (Biosciences, Ireland), 1% penicillin (100 U/ml), streptomycin (100 µg/ml) (Biosciences, Ireland) and amphotericin B (0.25 µg/mL) (Sigma-Aldrich, Ireland). All cells were maintained at 5% pO_2 during the expansion phase and the media changed twice weekly. BMSCs, FPSC, and chondrocytes were used at passage 2, 2 and 1 respectively. Porcine cells were used for *in vitro* experiments and for subcutaneous implantation in nude mice. Goat cells isolated from allogeneic tissues were used for implantation in caprine osteochondral defects.

2.3. Biofabrication of fibre-reinforced cartilage templates

A summary of the experimental procedure is shown in Fig. 1a. Custom built negative PLA moulds were fabricated using a 3D printer. 6% agarose was combined with 100 mM $CaCl_2$, pH 7.2, in a 1:1 ratio (final concentration of 3% and 50 mM respectively) and poured into the moulds to create cylindrical wells of diameter 6 mm and a height of 4 mm. To synthesise the RGD-γ alginate, low molecular weight sodium alginate (γ alginate, MW=58,000 g/mol) was prepared by irradiating sodium alginate (LF20/40, FMC Biopolymer) at a γ dose of 5 Mrad. Prior to RGD modification, γ alginate was oxidised by reacting sodium alginate with sodium periodate using a slight modification to a method previously reported [64]. γ alginate (10g) was dissolved in ultrapure deionised water (diH2O, 900 ml). Sodium periodate (0.1 g, Sigma) was dissolved in 100 ml diH2O, added to alginate solution under stirring to achieve 1 % theoretical alginate oxidation, and allowed to react in the dark at room temperature for 24 hrs. RGD-γ alginates were prepared by coupling the GGGGRGDSP to the oxidised γ alginate by carbodiimide reaction chemistry. To synthesise RGD-γ alginate, 2-morpholinoethanesulfonic acid (MES, 19.52 g, Sigma) and NaCl (17.53 g) were directly added to an oxidised alginate solution (1 L) and the pH was adjusted to 6.5. Sulfo-NHS (274 mg, Pierce, Rockford, IL), 1-Ethyl-3-(3-dimethylaminopropyl)carbodiimide (EDC, 484 mg, Sigma), and GGGGRGDSP peptide (100 mg, AIBioTech) were then added into the alginate solution. After reacting for 24 h at room temperature, the reaction was stopped by addition of hydroxylamine (0.18 mg/mL, Sigma), and the solution was purified by dialysis against ultrapure diH2O (MWCO 3500; Spectrum Laboratories) for 3 days, treated with activated charcoal (0.5 mg/100 mL, 50–200 mesh; Fisher, Pittsburgh, PA) for 30 min, filtered (0.22 mm filter), and lyophilised [7]. A reinforcing 3D printed polymer network was placed into each mould and 1.5% of RGD-γ alginate, containing 20 $\times$ 10^6 BMSCs/ml, was pipetted into the mould and allowed to cross-link at 37 °C for 30 min. All constructs were maintained in chondrogenic medium (CDM), consisting of hgDMEM supplemented with penicillin (100 U/ml)-streptomycin (100 µg/ml), 100 μg/ml sodium pyruvate, 40 μg/ml L-proline, 50 μg/ml L-ascorbic acid-2-phosphate, 1.5 mg/ml BSA, 1 $\times$ insulin-transferrin-selenium, 100 nM dexamethasone (all from Sigma-Aldrich, Ireland) and 10 ng/ml recombinant human transforming growth factor-β3 (TGF-β3; ProSpec-Tany TechnoGene Ltd, Israel). Constructs were cultured at 37 °C and 5% pO_2 for 28 days with medium exchange twice weekly.

2.4. Biofabrication of bi-phasic, PCL-reinforced cartilage templates

Orthogonal PCL architectures (12 mm diameter, 6 mm height, line spacing 2 mm) were printed with a tank and needle temperature of 70 °C, screw speed of 18 rev/s and a 30 gauge needle. The PCL was then punched using a 6 mm biopsy punch to form 6 $\times$ 6 mm unconfined lattice shaped constructs. The agarose-$CaCl_2$ moulds were fabricated using the same method as described above. However, two separate moulds were made with heights of either 6 mm or 4 mm. The experimental groups were fabricated as follows:

- *Single phase:* The PCL network was placed into the 6 $\times$ 6 mm agarose-$CaCl_2$ mould and 1.5% RGD-γ alginate containing 20 $\times$ 10^6 BMSCs/ml was pipetted into the mould up to the top and allowed to cross-link at 37 °C for 30 min.
- *Bi-Phasic Alginate*: The PCL network was placed into the 6 $\times$ 4 mm agarose-$CaCl_2$ mould. To form the 'osseous' (or 'endochondral') layer/phase, 1.5% RGD-γ alginate containing 20 $\times$ 10^6 BMSCs/ml was pipetted to the 4 mm height. The construct was left at 37 °C to cross-link for 10 min before being cut free and placed into the 6 $\times$ 6 mm agarose-$CaCl_2$ mould. To form the top 'chondral phase', 1.5% RGD-γ alginate containing 20 $\times$ 10^6 cells/ml of a 3:1 co-culture of FPSC:chondrocyte was used to form the top 2 mm of the construct. The constructs were cross-linked for a further 20 min before being cut free.
- *Bi-Phasic Agarose*: The PCL network was placed into the 6 $\times$ 4 mm agarose-$CaCl_2$ mould. To form the 'osseous' layer/phase, 1.5% RGD-γ alginate containing 20 $\times$ 10^6 BMSCs/ml was pipetted up to the 4 mm height. The construct

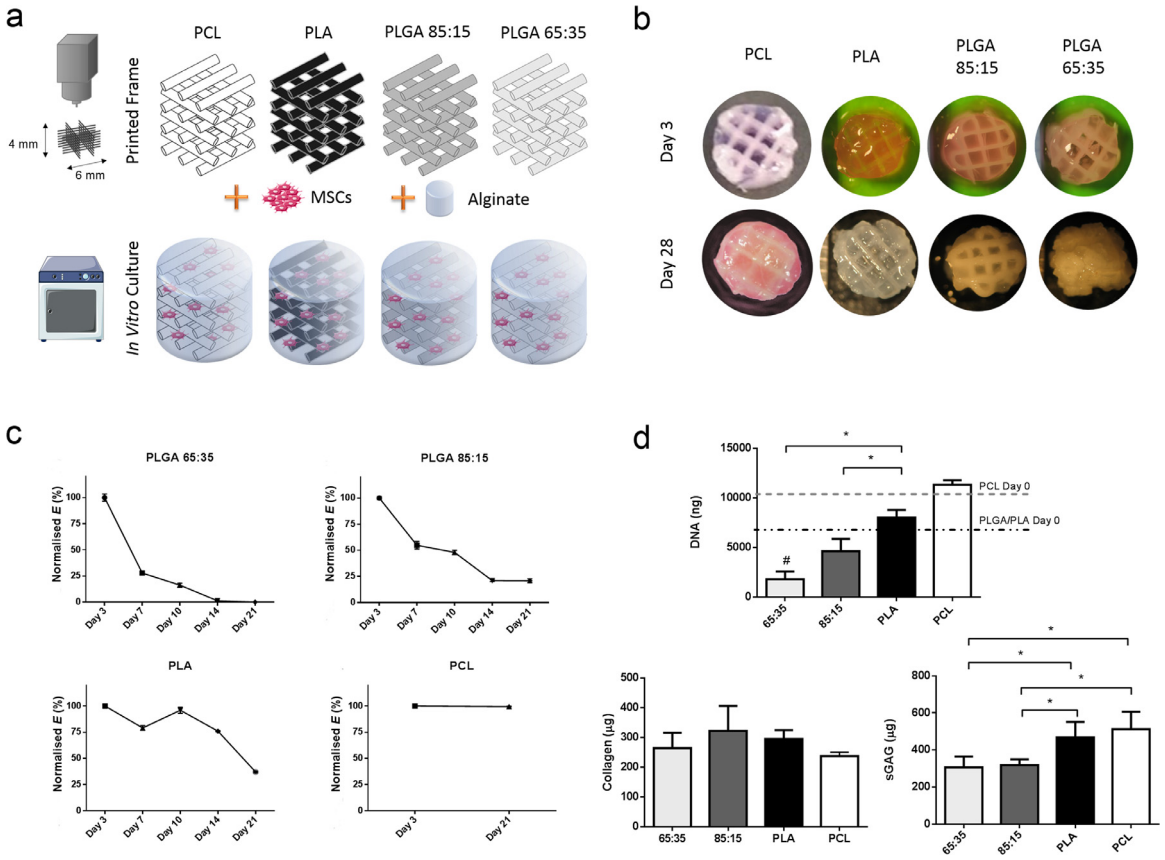

Fig. 1. a) Outline of the experimental groups, whereby 3D printed polymer frames were combined with cells encapsulated in alginate. b) Representative macroscopic plan view of the hybrid constructs after 3 and 28 days in culture. c) Young's modulus (E) normalised to day 0 of each experimental group. d) Biochemical analysis at day 28 for DNA, collagen and sGAG, $n = 3–4$, #significance compared to day 0, *significance, $p<0.05$.

was left to cross-link for 30 min before being cut free and placed into the 6 × 6 mm agarose mould. To form the 'chondral phase', 3% agarose type VI at a temperature of 42 °C was combined with 40 × 10^6 cells/ml of a 3:1 co-culture of FPSC:chondrocyte for a final agarose concentration of 1.5% containing 20 × 10^6 cells/ml. The agarose was allowed to gel for 10 min at room temperature before being cut free.

Bi-Phasic Self-assembly (SA): The PCL network was placed into the 6 × 4 mm agarose-$CaCl_2$ mould. To form the 'osseous' layer/phase, 1.5% RGD-γ alginate containing 20 × 10^6 BMSCs/ml was pipetted up to the 4 mm height. The construct was left to cross-link for 30 min before being cut free and placed into the 6 × 6 mm agarose mould. To form the 'chondral phase', 4 × 10^6 cells of a 3:1 co-culture of FPSC:chondrocyte in 100 μl of XPAN were pipetted on top of the 'osseous layer'. The cells were allowed to settle and aggregate in culture for a week (as described above) prior to the construct being cut free from the agarose mould.

2.5. Mechanical characterisation

Mechanical tests were performed using a single column Zwick (Zwick, Roell, Germany) with a 5 N load cell as previously described [65,66]. Briefly, stress relaxation tests were performed on constructs in XPAN media using impermeable metal plates. The Young's modulus was determined by measuring the slope of the stress-strain graph. The equilibrium compressive modulus was determined from the equilibrium force following unconfined compression testing to 10% strain.

2.6. Histology and immunohistochemistry

In vitro samples were fixed in 4% paraformaldehyde overnight before being embedded in paraffin and sliced at a thickness of 10 µm. *In vivo* samples were fixed in 10% formalin (Sigma-Aldrich, Ireland) for 3 days under agitation at room temperature. The samples were decalcified using 'Decalcifying Solution-Lite' (Sigma-Aldrich) for 1–6 weeks. Samples were frequently x-rayed to determine if any mineral content remained. When no mineral was visible, the sample was considered decalcified. The samples were cut along the longitudinal plane to be visualised, paraffin wax embedded and sectioned to a thickness of 10 µm. Slices were rehydrated through a graded series of xylenes and alcohols before being stained with 1% Alcian blue 8GX in 0.1 M HCl, pH 1 /Aldehyde Fuchsin or Safranin-O for sulfated glycosaminoglycan (sGAG), Picro Sirius Red for collagen and Haematoxylin and Eosin (H&E) (all Sigma-Aldrich, Ireland). Quantitative analysis was performed on multiple H&E-stained slices, whereby vessels (positive staining for endothelium and erythrocytes present within the lumen) were counted on separate sections taken throughout each sample and averaged for each sample. Collagen types I, II and X were evaluated using a standard immunohistochemical technique. Briefly, sections were treated with peroxidase, followed by treatment with chondroitinase ABC (Sigma–Aldrich) in a humidified environment at 37 °C to enhance the permeability of the extracellular matrix. Sections were incubated with goat serum to block non-specific sites and collagen type I (ab6308, 1:400, 1 mg/mL), collagen type II (ab3092, 1:100, 1 mg/mL) or collagen type X (ab49945, 1:200, 1.4 mg/mL) mouse monoclonal primary antibodies (Abcam, Cambridge, UK) were applied for 1 h at room temperature. Next

the secondary antibody (anti-mouse IgG biotin conjugate, 1:200, 2.1 mg/mL) (Sigma–Aldrich) was added for 1 h, followed by incubation with ABC reagent (Vectastain PK-400, Vector Labs, Peterborough, UK) for 45 min. Finally, sections were developed with DAB peroxidase (Vector Labs) for 5 min.

2.7. Biochemical analysis

Samples were digested in papain (125 μg/mL) in 0.1 M sodium acetate, 5 mM cysteine HCl, and 0.05 M EDTA (pH 6.0) (all from Sigma-Aldrich) at 60 °C under constant rotation for 18 h. Total DNA content was quantified using the Hoechst Bisbenzimide 33,258 dye assay (Sigma-Aldrich). sGAG content was quantified using the dimethylmethylene blue dye-binding assay (Blyscan, Biocolor Ltd.) pH 1.35, with a chondroitin sulfate standard. Calcium content was analysed by digesting the samples in 1 M of HCL at 60 °C under constant rotation until sample was fully dissolved. Calcium was detected using the sentinel calcium kit (Alpha Labs, UK). Total collagen content was determined by measuring the hydroxyproline content. Samples were hydrolysed at 110 °C for 18 h in concentrated HCL (38%) and assayed using a chloramine-T assay with a hydroxyproline-to-collagen ratio of 1:7.69.

2.8. Micro-computed tomography (μCT)

μCT scans were performed using a Scanco Medical 40 μCT system (Scanco Medical, Bassersdorf, Switzerland) to visualise and quantify mineral deposition. Constructs were scanned in 50% EtOH, at a voxel resolution of 30 μm, a voltage of 70 kVp, and a current of 114 μA. Reconstructed 3D images were generated to visualise the repaired bone. Quantification of mineralization within the defect site was performed by setting a threshold of 210 (corresponding to a density of 399.5 mg hydroxyapatite/cm^3).

2.9. Surgical procedures

2.9.1. Mouse surgery

Following 5 weeks *in vitro* priming, the bi-phasic constructs ($n = 6$ per group) were implanted subcutaneously into the back of nude mice (Balb/c; Harlan, UK). Two subcutaneous pockets were created at the shoulders and the hips and then three constructs were inserted per pocket. Mice were sacrificed 6 weeks post-implantation by CO_2 inhalation. The animal protocol was reviewed and approved by the ethics committee of Trinity College Dublin and the Irish Medicines Board (AE19136/P026).

2.9.2. Goat surgery

Following 4 weeks *in vitro* priming, the bi-phasic constructs were implanted into the medial femoral condyle of skeletally mature goats. The surgical procedure in the caprine model was performed as previously described [67]. Briefly, following anaesthesia, an arthrotomy of each stifle joint was performed using the lateral para-patellar approach. A critically-sized defect, 6 mm in diameter x 6 mm in depth, was created in each site using a hand drill, a flattened drill bit and a depth guide. The joint was flushed with fluids (0.9% NaCl) and the defect filled with a bi-phasic self-assembly implant ($n = 6$). Euthanasia was carried out at 6 months to permit harvesting of the treated regions. Repair was compared to that observed in a parallel study in the same animal model [68], where defects were treated with the Maioregen scaffold (Finceramica), which is herein referred to as the control scaffold ($n = 8$). Ethical evaluation and approval was performed by University College Dublin (AREC 12–71) and the Irish Government Department of Health (B100/4517).

2.10. Evaluation of cartilage repair within goat joints

Histological scoring on H&E and Safranin-O stained samples was carried out according to an assessment criteria adapted from the International Cartilage Repair Society (ICRS) (Supplementary Table S1). Histomorphometry was performed on sections stained with Safranin-O using Photoshop CS6 whereby the number of pixels of red colour were quantified and normalised to the total number of pixels in the image [68]. Picro Sirius Red stained samples were imaged under polarised light microscopy (PLM) to investigate collagen fibre orientation and Image J software was used to quantify the average orientation of the collagen fibres and provide a dispersion value for the distribution using the directionality function [69].

2.11. Statistical analysis

Results are presented as mean ± standard deviation. Statistical analysis was performed with GraphPad Prism 6 software package (GraphPad, USA). Unless otherwise stated, experimental groups were analysed for significant differences using a general linear model for analysis of variance (ANOVA) and Tukey's post-test. Significance was accepted at a level of $p < 0.05$.

3. Results

3.1. Engineered cartilaginous tissues mechanically reinforced with networks of 3D printed PCL, PLA or PLGA

BMSC-laden alginate hydrogels were mechanically reinforced using networks of 3D printed PCL, PLA or PLGA fibers (Fig. 1a,b), and then maintained in chondrogenic culture for 28 days. There was no change in the PCL filament diameter (0.22±0.03 mm) over 28 days *in vitro* nor was there a change in the mechanical properties of printed PCL networks over 21 days *in vitro* (Fig. 1c). In contrast, the PLGA fibres were observed to swell over the time in culture (Fig. 1b; Supplementary Fig. S1). By day 14 it was not possible to measure the fibre diameter of PLGA 65:35 constructs and by day 28 the cylindrical geometry was unrecognisable from that originally printed (Fig. 1b). The PLGA 65:35 failed to provide mechanical reinforcement with time in culture, with the Young's modulus reducing from 7.17 MPa to 0.0075 MPa by day 21 (Fig. 1c). The mechanical properties of the PLA and the PLGA 85:15 constructs underwent less dramatic changes in mechanical properties over time in culture, reducing in Young's moduli from 15.31 MPa to 5.6 MPa for the PLA constructs, and from 11.4 MPa to 2.375 MPa for the PLGA 85:15 constructs (Fig. 1c). The PLGA 85:15 constructs better maintained their structure, although the printed fibres did swell by 28% from day 3 to 28 (Supplementary Fig. S1), with the final strut size measured as 0.59 mm. Overall the fibers in PLA reinforced constructs maintained their fibre diameter during the 28 days in culture.

We next assessed chondrogenesis of BMSCs encapsulated within these fibre-reinforced alginate hydrogels. Over 28 days in culture, DNA levels significantly reduced in the PLGA 65:35 constructs (Fig. 1d), suggesting a loss of cell viability over time, likely due to the acidic PLGA degradation by-products. No significant drop in DNA content was observed in the PLGA 85:15 constructs. No significant difference in DNA levels were observed over time in the PLA and PCL constructs, and both supported significantly higher levels of sGAG synthesis than constructs reinforced with PLGA (Fig. 1d). All engineered tissues stained positive for sGAG and type II collagen deposition (Supplementary Fig. S2). PCL had higher DNA at day 0 (9137±931 ng) compared to the PLA and PLGA groups (6766±64 ng). This may be a result of the thinner fibres of PCL allowing a greater area for hydrogel infiltration. As

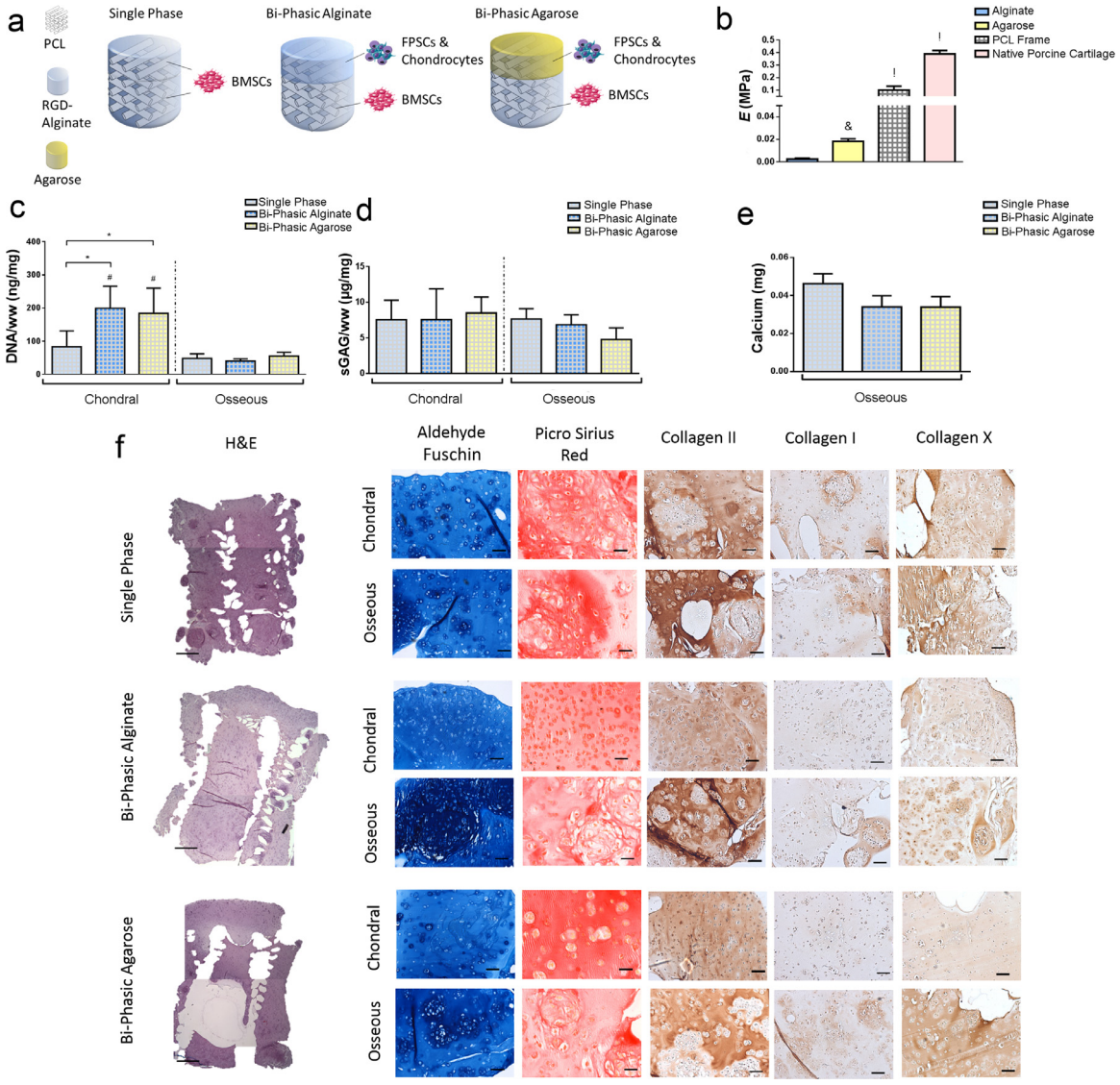

Fig. 2. a) Overview of experimental groups. b) Young's Modulus (E) for acellular alginate and agarose, PCL frame and 3-month old porcine cartilage, n = 3–4, & significance compared to alginate, ! significance compared to all other groups, $p<0.05$. c) DNA/ww. d) sGAG/ww (*significance, # significance compared to the corresponding osseous layer, $p<0.05$, n = 6, e) Calcium content. f) Staining of histological sections for H&E, scale bar =1 mm, and Aldehyde Fuchsin, Picro Sirius Red and collagen types II, I and X, scale bar=200 μm.

superior chondrogenesis was observed in the PLA and PCL scaffolds, and given that PCL could be printed at lower temperatures and hence is more compatible with bioprinting strategies, PCL was used as a reinforcing network for both the osseous/endochondral phase and chondral phase of osteochondral constructs described in the remainder of this study.

3.2. In vitro *evaluation of fibre-reinforced, bi-phasic cartilage templates*

In an attempt to engineer bi-phasic hydrogels capable of spatially supporting either endochondral bone (bottom layer/phase) and articular cartilage (top layer/phase) development, the bottom osseous region of 3D printed scaffolds was first loaded with alginate hydrogel containing BMSCs. Next, the top chondral region was loaded with either an alginate (hereon in termed '*Bi-Phasic Alginate*') or agarose (hereon in termed '*Bi-Phasic Agarose*') hydrogel containing a co-culture of chondrocytes and FPSCs (Fig. 2a). To engineer fibre-reinforced hydrogels with mechanical properties mimicking that of articular cartilage, the top chondral region contained a printed PCL network with a larger filament spacing of 2 mm. The Young's modulus of these PCL networks was dramatically higher than that of agarose and alginate alone, of a similar order of magnitude to that of native articular cartilage (Fig. 2b). Control constructs consisted of single-phase alginate hydrogels that were also reinforced with PCL networks and seeded throughout with BMSCs (hereon in termed '*Single Phase*'; Fig. 2a). After 5 weeks of *in vitro* culture in chondrogenic conditions, DNA levels (normalised to tissue wet weight) were significantly higher in the chondral region of bi-phasic alginate and agarose constructs compared to their osseous region and to the same region within single phase controls (Fig. 2c). No significant differences in overall levels of sGAG deposition were observed between the osseous and chondral region of bi-phasic constructs (Fig. 2d). Calcium was detected in small amounts in the osseous region of all groups (Fig. 2e). H&E staining of bi-phasic alginate and agarose constructs demonstrated seamless integration between chondral and osseous regions, with the 3D printed PCL framework (subsequently removed by xylene immersion during histological processing) evident throughout both osseous regions (Fig. 2f). Robust chondrogenesis was confirmed in

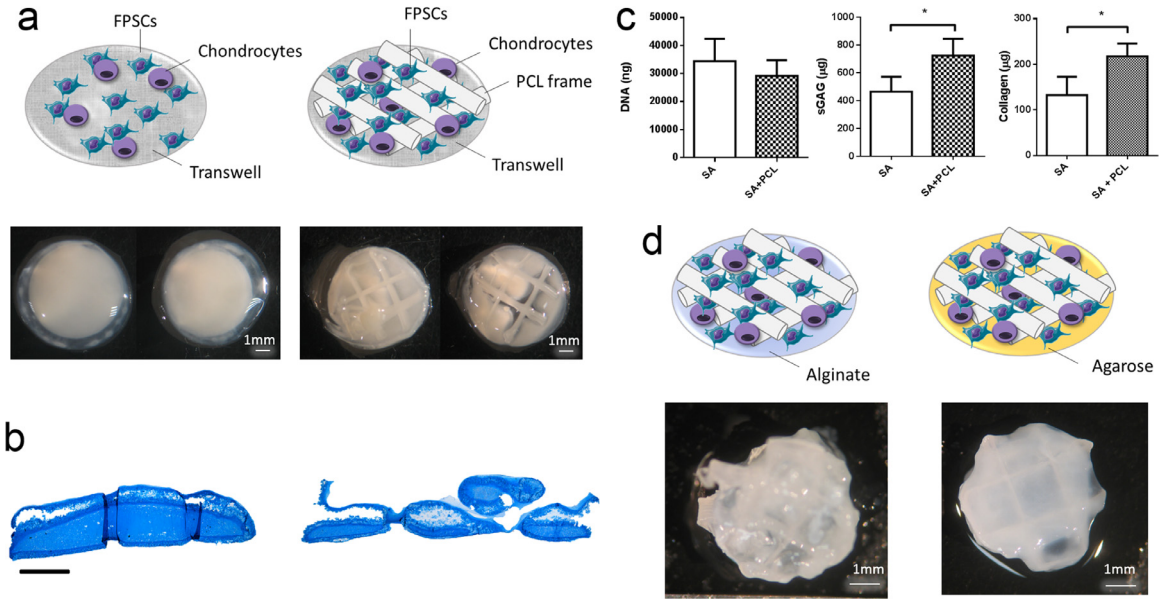

Fig. 3. Cartilaginous tissues engineered by SA of chondrocytes and FPSCs. a) Schematic of experimental groups and macroscopic images after 6 weeks of *in vitro* culture. b) Alcian blue staining for sGAG of SA (left) and SA + PCL (right) after 6 weeks of *in vitro* culture. Scale bar 1 mm. c) Biochemical analysis for DNA, sGAG and collagen, $^{*}p<0.05$, d) Schematic of experimental groups and macroscopic images after 6 weeks of *in vitro* culture.

all groups through positive staining for Aldehyde Fuchsin and collagen type II (Fig. 2f). The chondral region of single phase constructs stained more intensely for collagen types I and X compared to the corresponding regions in both bi-phasic constructs, indicating progression towards hypertrophy in the chondral region of the single phase group.

As an alternative to hydrogel encapsulation to form the chondral layer of these bi-phasic implants, we also explored the use of a self-assembly (SA) or scaffold-free approach to generate stable articular cartilage, as previous studies have demonstrated that such SA approaches can facilitate the development of a more structurally organised engineered tissue [70]. By loading a defined numbers of cells (same chondrocyte & FPSC co-culture as described above) alongside 3D printed PCL fibers (Fig. 3a), we confirmed that the presence of these fibers did not negatively interfere with the capacity of cells to self-assemble and generate a surface layer of articular cartilage (Fig. 3b). In fact, total sGAG and collagen deposition was higher in the presence of the 3D printed fibers (Fig. 3c). We also confirmed that such SA tissues can be formed on the surface of either alginate or agarose hydrogels reinforced with 3D printed PCL networks (Fig. 3d). This allows us to generate the chondral layer of our bi-phasic constructs using either hydrogel encapsulation or SA.

3.3. In vivo *evaluation of fibre-reinforced, bi-phasic cartilage templates following subcutaneous implantation in nude mice*

Following 5 weeks of chondrogenic priming, all constructs (Single Phase, Bi-Phasic Alginate, Bi-Phasic Agarose, Bi-Phasic SA) were implanted subcutaneously into nude mice (Fig. 4a). 6 weeks after subcutaneous implantation, an obvious interface had formed between the osseous and chondral layers of the bi-phasic constructs (Fig. 4b). The bone region contained visible vasculature, whereas the cartilage had a white hyaline cartilage-like appearance and appeared avascular. This observation was supported by μCT analysis, which demonstrated negligible mineral deposition in the chondral layers of bi-phasic constructs compared to the single-phase control (Fig. 4c). Quantification of mineral deposition confirmed that the chondral region of the single-phase implants contained a significantly higher amount of mineral compared to all bi-phasic constructs (Fig. 4d). A large number of blood vessels were detected in the osseous regions of all constructs, indicating that the mineralised cartilage tissue was vascularised (Fig. 4b). Significantly fewer vessels were detected in the chondral phase, with a trend towards a larger number of vessels being detected in this region of the single-phase control implant (Fig. 4e). Histological analysis confirmed that the bi-phasic constructs supported spatially defined tissue types *in vivo*. H&E staining demonstrated the development of a vascularized, bone-like tissue confined to the osseous region of the bi-phasic constructs, and in pockets throughout all regions of the single phase control constructs (Fig. 4f). The chondral region of the bi-phasic constructs contained a cartilage-like tissue, as evident by positive staining for sGAG and type II collagen deposition (Supplementary Fig. S3). The chondral regions also stained positive for type I and X collagen deposition, although generally less so than the corresponding osseous regions of the same constructs.

3.4. *Treatment of caprine osteochondral defects with fibre-reinforced, bi-phasic cartilage templates*

Having verified that we could engineer mechanically reinforced, spatially defined tissues in a subcutaneous environment, we next sought to evaluate the capacity of these engineered cartilage templates to direct regeneration of critically sized osteochondral defects in a caprine model. Following chondrogenic priming, reinforced bi-phasic SA constructs were implanted into critically sized defects in the medial condyle of skeletally mature goats (Fig. 5a). 6 months after implantation, the repair tissue was analysed by staining with Safranin-O for proteoglycans and for collagen type II deposition (Fig. 5b). Most of the cartilage template within the osseous region of implants appeared to have undergone endochondral ossification, as evident by limited Safranin-O staining in the bony region of defects, being replaced with cancellous bone. In some cases, there was evidence of remnant implant material in the bony region of the defect. In the worst-case outcome (one animal), the defect and implant appeared to have collapsed inward, suggesting insufficient integration and/or mechanical stability of the implant. It should be noted that cases of defect collapse were

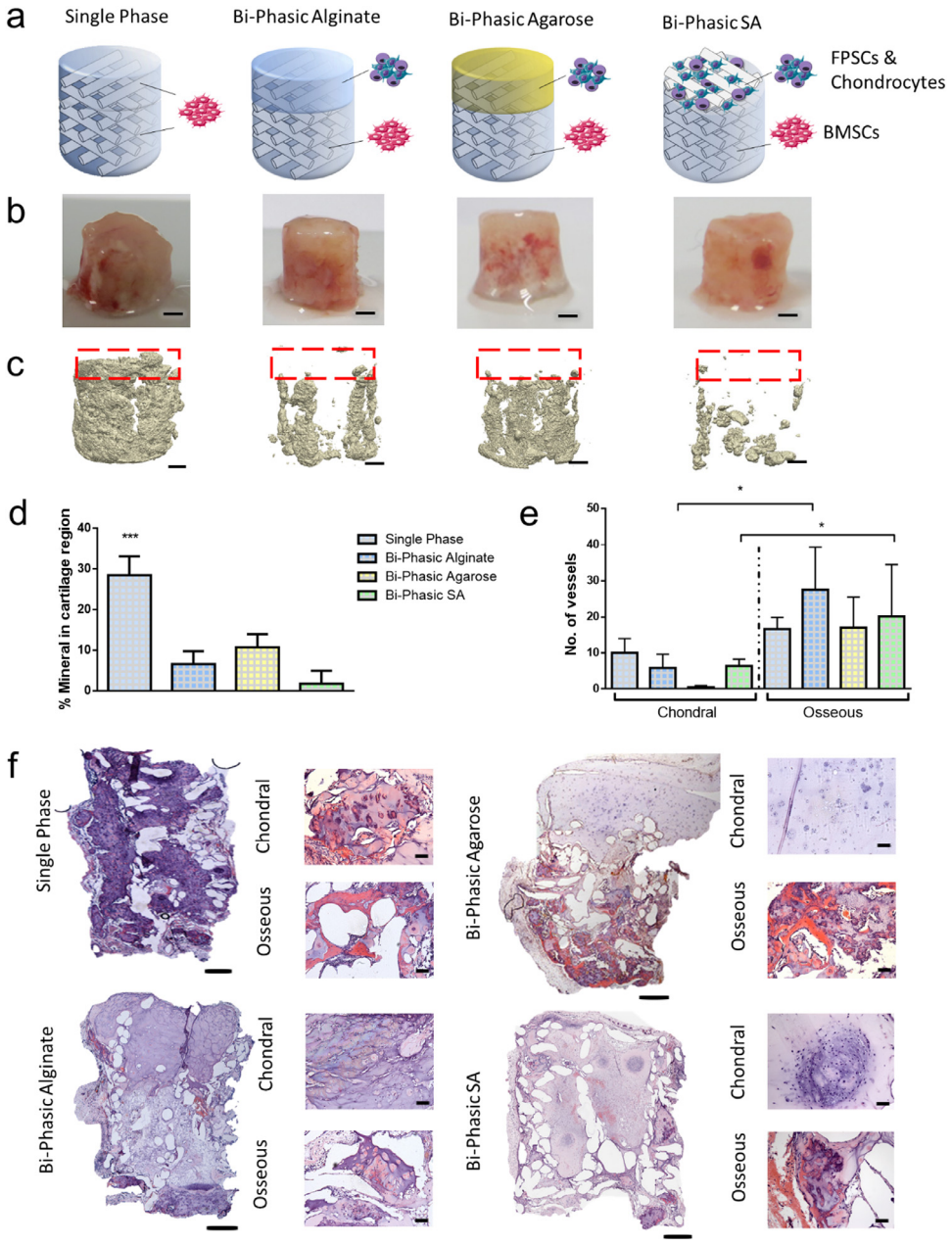

Fig. 4. a) Schematic of the groups implanted into the nude mice. b) Representative macroscopic images post-implantation in nude mice (scale bar 1 mm). c) µCT 3D renderings demonstrating mineral deposition in each group, the red box signifies where the chondral region is located (scale bar 1 mm). d) Quantification of the mineral volume from the µCT shown as the percentage of overall mineral that was detected in the chondral region, ***significance $p<0.05$ compared to all other groups. e) The number of vessels in the chondral and osseous regions (from H&E sections) *significance $p<0.05$. f) H&E staining, main image scale bar 1 mm, inset image scale bar 100 µm.

also observed in the control group. The area within the chondral and osseous regions of defects staining positive for Safranin-O was quantified, which revealed a trend towards higher levels of cartilage tissue formation within the chondral region of defects treated with bi-phasic SA constructs (Fig. 5c). Significantly higher amounts of cartilage tissue were found in the chondral region compared to the osseous region of defects treated with bi-phasic implants; this spatial difference was not observed in defects treated with control scaffolds, confirming the potential of these engineered implants to spatially direct tissue development within load bearing defects. The orientation of the collagen fibres within the cartilage regions of the newly formed tissue was next analysed using polarised light microscopy (Fig. 5d). The angle of orientation in the superficial (top) and the bottom regions were determined and compared to native controls. Treatment with the bi-phasic construct resulted in a more favourable parallel fibre orientation (~0°) and a lower dispersion rate compared to the control scaffold in the superficial region of the defect (Fig. 5e). In both groups the bottom region of the tissue had more varied results, however overall the newly synthesised tissue resulting from treatment with the SA bi-phasic construct resulted in a more native-like perpendicular fibre orientation (90°) (Fig. 5e).

We next sought to assess the quality of the repair tissue formed within the defects. To that end, we performed histological scoring adapted from the ICRS system (Fig. 6). In a number of categories, no significant differences were observed between defects treated with control scaffolds and defects treated with engineered bi-phasic SA tissues (Fig. 6a, d, e, f, j, k, l, m). However, defects

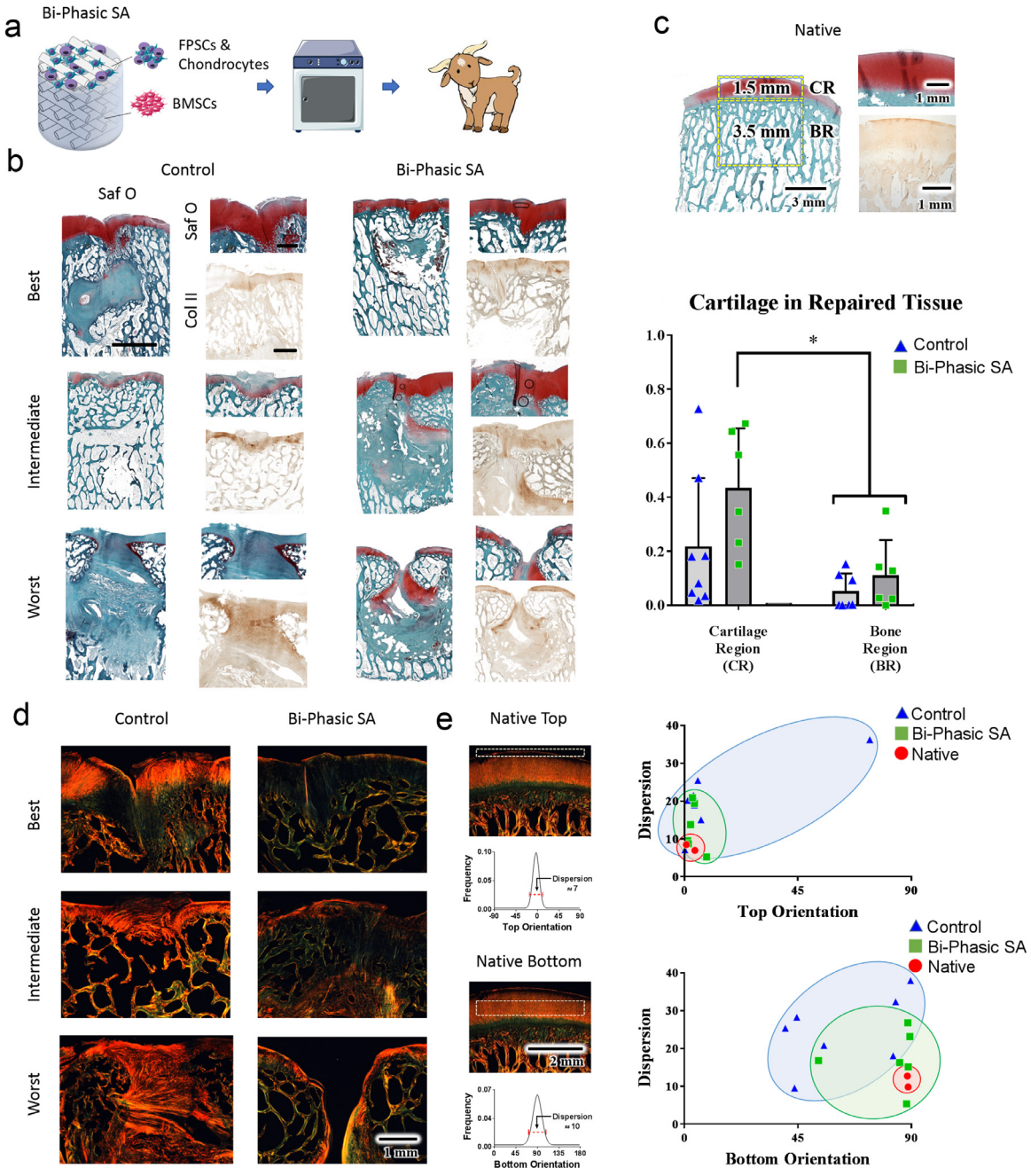

Fig. 5. a) Schematic of the experiment. b) Histological sections stained with Safranin-O for sGAG detailing the repair with the bi-phasic scaffold compared to the control scaffold. Main image scale bar 3 mm. Inset image scale bar 1 mm c) A native condyle depicting the regions assessed by histomorphometry whereby the cartilage in the repaired tissue was quantified by normalising the area of positive Safranin-O staining to the total area of the region ($p<0.05$). d) Polarised light microscopy. e) Dispersion of the collagen fibres within cartilage regions.

treated with bi-phasic SA tissues demonstrated a significant increase in matrix staining compared to defects treated with control scaffolds (Fig. 6b) (81± 23 vs. 40 ± 34.8; $p = 0.0318$). Furthermore, bi-phasic SA tissues were observed to score significantly higher in terms of cell morphology when compared to control scaffolds (Fig. 6c) (85 ± 8.5 vs. 54 ± 28; $p = 0.0265$). A number of trends towards significance were also observed, with the bi-phasic SA group scoring higher in the abnormal calcification (Fig. 6h) ($p = 0.0816$) and superficial assessment (Fig. 6i) ($p = 0.1$) categories, whilst the control scaffold group was found to score higher in the subchondral bone abnormalities category (Fig. 6g) ($p = 0.0514$). Taken together, these results would appear to demonstrate an improvement in the repair process within osteochondral defects treated with bi-phasic scaffolds, resulting in the generation of a more hyaline-like cartilage tissue.

4. Discussion

The overall aim of this study was to engineer fibre-reinforced cartilage templates for osteochondral defect repair, whereby the osseous region of the implant is designed to undergo endochondral ossification, whilst the overlying chondral layer is designed to support the development of stable hyaline cartilage. To achieve this goal, 3D printing was used to produce polymer networks to mechanically reinforce cell-laden hydrogels, while different combinations of cells and biomaterials were evaluated for their capacity

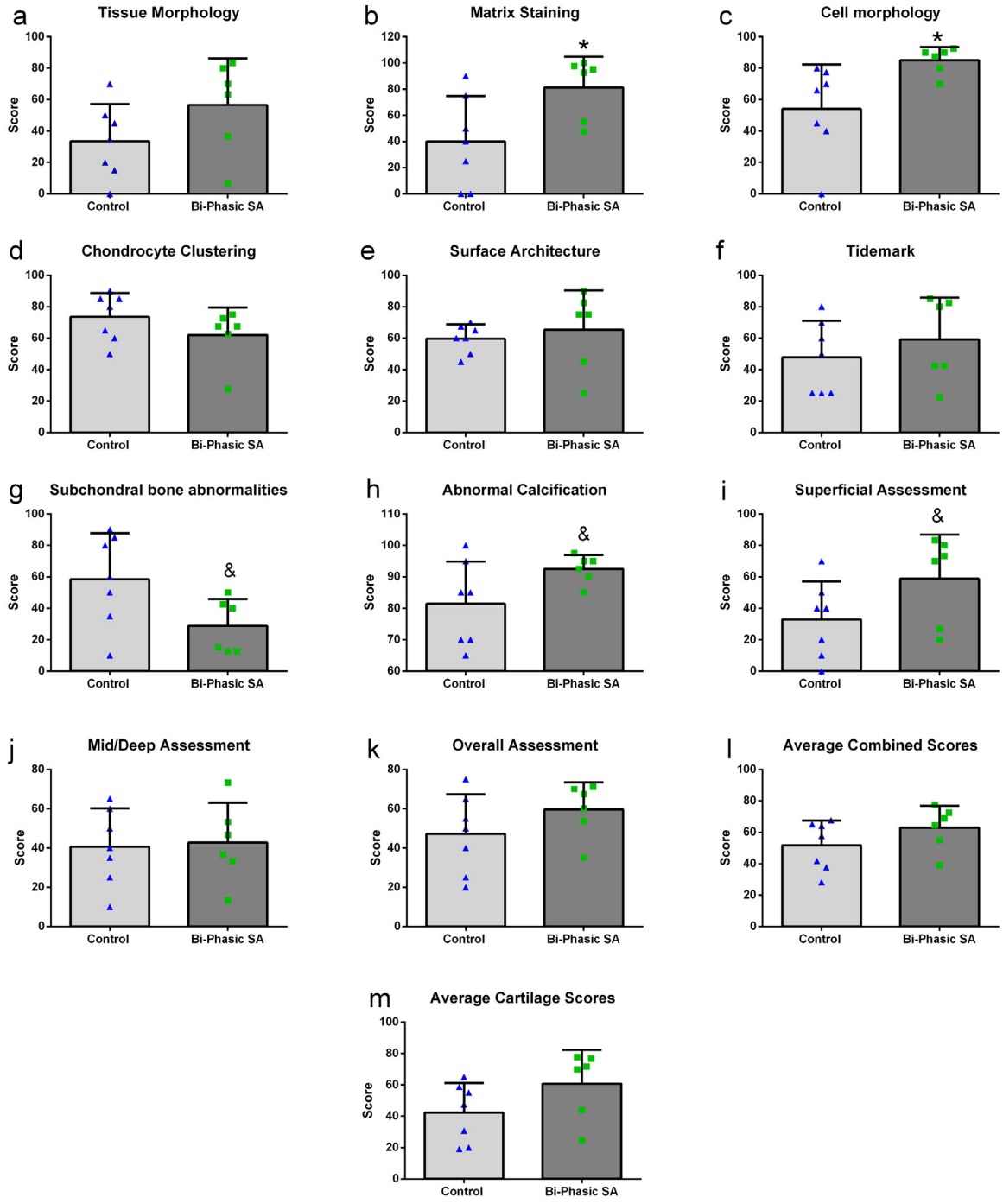

Fig. 6. ICRS scores for defects treated with either control scaffolds or bi-phasic scaffolds. Average Cartilage Scores (m) were defined as the average of the ICRS scores related to the chondral region specifically (*i.e.* a, b, e, i, j and k). Significance; & $p \leq 0.1$, * $p<0.05$ compared to control group as determined by *t*-test.

to support either stable cartilage or endochondral bone development. We demonstrated that hydrogels could be mechanically reinforced using different 3D printed thermoplastics (PLA, PLGA 65:35, PLGA 85:15 and PCL), to generate composite constructs capable of supporting robust chondrogenesis. Reinforced bi-phasic cartilage templates were next engineered, where the articular cartilage layer was engineered using a co-culture of chondrocytes and stem cells. The co-culture supressed calcium deposition and markers of hypertrophic differentiation in the chondral layer *in vitro*. 6 weeks after subcutaneous implantation, a clear distinction between the chondral and osseous layers of the bi-phasic implants was observed, with blood vessels generally confined to the lower osseous half of the construct. Micro CT, vessel quantification and histological staining confirmed this finding, with mineralised bone restricted to the osseous layers, confirming that the co-culture was supressing vascularisation and mineralisation of the chondral layer. Finally, chondrogenically primed bi-phasic constructs were implanted into critically sized osteochondral defects to assess their regenerative potential in a clinically relevant environment. Treatment of these defects with bi-phasic constructs resulted in

a more hyaline-like cartilage repair compared to defects treated with control scaffolds, as evidenced by a collagen fibre architecture more akin to native cartilage.

Scaffolds produced using 3D printed PLA, PLGA 85:15 and PLGA 65:35 all experienced a loss in mechanical properties over time. Numerous studies have explored the degradation of PLA and PLGA, describing how the mechanical properties can be tuned based on the method of manufacture and the polymer molecular weight. For example, an ester end cap PLGA will degrade more slowly than an acid end cap [49]. There are a number of factors which may have contributed to the rapid degradation of the PLGA scaffolds observed in this study. Forming scaffolds through printing has been shown to decrease the polymer molecular weight, which can speed up the degradation process [60]. Additionally, the sterilisation method can affect the surface of the PLGA, creating cracks and pores [71,72]. In this case, the scaffolds were sterilised by ETO gas. In a study comparing the effects of common sterilisation methods on PLGA 75:25, it was revealed that ETO treatment resulted in 12% decrease in polymer molecular weight [71].

The fibre patterns used in this study were selected in order enhance the mechanical properties of the scaffold whilst simultaneously ensuring a sufficient porosity so as to facilitate the inclusion of cell-laden hydrogels and the subsequent deposition of cartilaginous matrix. Although the initial mechanical properties of the scaffolds are lower than that of bone, they are robust when handling and easily support the inclusion of cell-laden hydrogels. PLA and PCL reinforced hydrogels supported the highest levels of chondrogenesis whilst maintaining mechanical and structural integrity. It is possible that the acidic environment created by PLGA degradation products is causing cell death [63] and/or impeding chondrogenesis. It should be noted, however, that several studies have reported that PLGA supports MSC proliferation over time [73– 75], although in general these studies do not explore long-term cell fate *in vitro* as undertaken here.

PCL was chosen over PLA due to its lower printing temperature (for future co-printing potential) and more elastic mechanical properties. PLA has a high glass transition temperature (approximately 60–65°C) causing it to be brittle [49,76]. It has been reported that PLGA/PLA degrades faster *in vivo* than *in vitro*, therefore it may not be stable enough in a load bearing joint [77]. Improvements can be made by increasing the molecular weight of the PLA/PLGA or by blending it with PCL [76,78–80]. For example, PCL-PLGA-β-tricalcium phosphate was used to promote bone formation in a lapine calvarial defect model [78]. Another study examining electrospun blends of PCL and PLGA demonstrated a reduced strain at failure during tensile testing, and such properties could be modified based on the ratio of components. Importantly, elastic and plastic regions were increased [80]. However, further studies would need to be performed on the compressive properties of this material and the degradation over time.

A co-culture of FPSCs and chondrocytes appeared to support the development of more hyaline-like cartilage *in vitro*. Whilst overall levels of sGAG accumulation did not increase in tissues engineered using such co-cultures, there was a significant increase in their DNA content. Several studies have demonstrated that MSCs secrete factors such as FGF-1, FGF-2, TGF-β3 and IGF-1 [81–83] that drive the proliferation of chondrocytes [84–86]. Both calcium and collagen type I were present in the MSC-laden osseous regions and in the homogenous alginate-PCL controls, however there was no such staining observed in the chondral regions that were engineered using a co-culture of chondrocytes and stem cells. Taken together, these results suggest that cartilaginous tissues engineered using co-cultures of chondrocytes and stem/progenitor cells may be an effective cell-based therapy for articular cartilage repair, as only a relatively small of chondrocytes are needed to engineer phenotypically stable cartilage. Indeed, these engineered tissues could act as an alternative to current treatments such as autologous chondrocyte implantation, which require chondrocytes to be expanded extensively *in vitro* which can result in de-differentiation into a more fibrogenic phenotype [87].

An advantage of utilising bi-phasic cartilaginous templates for osteochondral tissue engineering is that both phases of the construct can be maintained in the same chondrogenic culture conditions *in vitro*, as the approach relies on the cells within the two phases executing opposing programs *in vivo*. Following subcutaneous implantation, distinct tissues developed *in vivo* within the different regions of the bi-phasic implants. Vasculature was clearly evident in the lower portion of the construct, with a white, avascular hyaline cartilage-like tissue forming on the top surface. The two layers were well integrated, appearing very much like an osteochondral plug. The co-culture suppressed mineralisation *in vivo*, with the upper portion devoid of mineral in μCT scans. However, there was no distinct difference between the chondral regions engineered using self-assembly, agarose or alginate hydrogels. Given that the self-assembly approach reduces concerns with regards to material degradation in the cartilage layer, a SA bi-phasic construct was selected to be implanted into the caprine osteochondral defect and was compared to data generated using a market leading multi-layered scaffold [68] which has previously been shown to promote osteochondral regeneration over empty defects [88].

6 months after implantation, the reinforced bi-phasic SA construct promoted hyaline-like cartilage repair in the majority of animals. The zonal collagen structure plays a key role in determining the mechanical properties of articular cartilage [89], which is imperative to a functioning joint. This structure was seen more consistently in the joint repaired with the bi-phasic construct and was accompanied by an enhancement in cartilage matrix synthesis in the region. Further improvements in the quality of cartilage repair might be possible with longer and/or more complex culture conditions to engineer a more functional articular cartilage layer prior to implantation. Of concern was the observation that the quality of subchondral bone repair in defects treated with bi-phasic scaffolds was inconsistent. Both the PCL and alginate materials used in the development of this tissue engineered implant have been used previously *in vivo* and proven to be biocompatible [7,90]. In some cases there was evidence of residual implant material, although whether this is impacting bone healing is unclear. It's possible that alternative printing techniques, such as melt electrowriting [91], which allow for the generation of fibre networks with lower volume fractions may be of benefit in this regard [48]. Tailoring the material degradation rate to facilitate vascularization and host cell invasion is critical for robust bone formation. Materials which do not degrade quickly can delay bone formation by occupying space needed by the cells to deposit ECM [8]. The alginate in this system was γ-irradiated, which has been shown to support superior bone tissue formation compared to non-irradiated alginate [7]. Finally, in one animal it appeared that the defect completely collapsed, suggesting failure of the implant to integrate with the surrounding tissue and/or provide adequate mechanical support to the defect.

Alternative strategies could be leveraged to promote more robust bone formation within the osseous component of these implants and to ensure better implant integration. Future studies could, for example, focus on enhancing the osteogenic potential of the osseous layer by inducing channels or canals [92] which would more closely mimic and direct the endochondral ossification process [21,93]. Canals are formed during endochondral ossification and are thought to serve three primary functions; metabolic exchange, the supply of osteogenic cells and to act as a reservoir of cells for cartilage growth [93]. Such channels could be formed using the 3D printing software, whereby sacrificial materials such as gelatine, sucrose or pluronic could be printed in the desired canal architecture and subsequently washed away following cross-linking

of the cell seeded bioink [94–97]. Another approach may be to incorporate growth factors such as bone morphogenetic protein-2 or vascular endothelial growth factor through loading onto polymers or encapsulation into degradable microspheres [98]. A further more complex strategy may be to utilise the concept of the '*in vivo* bone bioreactor' [99] to enable maturation of engineered osteochondral unit in an ectopic location prior to implantation into an orthotopic defect. This system was described in a seminal paper by Stevens et al., and functions by using a space between the periosteum and the tibia to stimulate growth of a cell-seeded hydrogel. After 6 weeks, mature bone had been formed, it could be harvested from the '*in vivo* bioreactor' and used as a graft to repair a bone defect. The process was also demonstrated as viable for the engineering of articular cartilage [99]. Finally, it should be noted that allogenic caprine cells were used in this study. While these implants were well tolerated by the animals, the lack of an earlier time point to assess for a possible immune response to the implanted allogeneic cells can be considered a limitation of the study. It also remains technically challenging to determine whether *de novo* tissue formed within the defect site is of donor or host origin in such longer-term large animal studies.

To conclude, this work investigated the possibility of engineering a mechanically reinforced, bi-phasic construct capable of promoting regeneration of a critically sized osteochondral defect. To this end, an iterative approach was executed in order to determine the appropriate combinations of cells and biomaterials to be utilised within this bi-phasic construct. Ultimately, a bi-phasic construct consisting of a self-assembled MSC-chondrocyte tissue, layered on top of an MSC-laden alginate hydrogel, and reinforced throughout with a PCL fibre network, was evaluated *in vitro* and *in vivo* and was found to facilitate the regeneration of hyaline-like cartilage within critically sized caprine osteochondral defects. Examples of implant failure *in vivo* also point to the need for further improvements in the design of these constructs. Together these findings motivate the continued development of reinforced bi-phasic cartilage implants as soft tissue templates for osteochondral regeneration.

Declaration of Competing Interest

None.

Acknowledgements

Funding was provided by Science Foundation Ireland (12/IA/1554). We would also like to acknowledge the support of staff within the Comparative Medicine Unit in Trinity College Dublin for their help with the nude mouse model and the members of the school of Veterinary Medicine, University College Dublin for their help with the goat model.

Supplementary materials

Supplementary material associated with this article can be found, in the online version, at doi:10.1016/j.actbio.2020.05.040.

References

[1] K.L. Spiller, S.A. Maher, A.M. Lowman, Hydrogels for the repair of articular cartilage defects, Tissue Eng. Part B Rev. 17 (4) (2011) 281–299.
[2] E.J. Sheehy, T. Mesallati, T. Vinardell, D.J. Kelly, Engineering cartilage or endochondral bone: a comparison of different naturally derived hydrogels, Acta Biomater. 13 (2015) 245–253.
[3] T. Mesallati, C.T. Buckley, D.J. Kelly, A comparison of self-assembly and hydrogel encapsulation as a means to engineer functional cartilaginous grafts using culture expanded chondrocytes, Tissue Eng. Part C: Methods 20 (1) (2014) 52–63.
[4] E.J. Sheehy, T. Mesallati, L. Kelly, T. Vinardell, C.T. Buckley, D.J. Kelly, Tissue engineering whole bones through endochondral ossification: regenerating the distal phalanx, Biores Open Access 4 (1) (2015) 229–241.
[5] T. Mesallati, C.T. Buckley, D.J. Kelly, Engineering cartilaginous grafts using chondrocyte-laden hydrogels supported by a superficial layer of stem cells, J. Tissue Eng. Regen. Med. 11 (5) (2017) 1343–1353.
[6] H.A. Awad, M.Q. Wickham, H.A. Leddy, J.M. Gimble, F. Guilak, Chondrogenic differentiation of adipose-derived adult stem cells in agarose, alginate, and gelatin scaffolds, Biomaterials 25 (16) (2004) 3211–3222.
[7] E. Alsberg, H.J. Kong, Y. Hirano, M.K. Smith, A. Albeiruti, D.J. Mooney, Regulating bone formation via controlled scaffold degradation, J. Dent. Res. 82 (11) (2003) 903–908.
[8] G.M. Cunniffe, T. Vinardell, E.M. Thompson, A.C. Daly, A. Matsiko, F.J. O'Brien, D.J. Kelly, Chondrogenically primed mesenchymal stem cell-seeded alginate hydrogels promote early bone formation in critically-sized defects, Eur. Polym. J. 72 (2015) 464–472.
[9] J.L. Drury, D.J. Mooney, Hydrogels for tissue engineering: scaffold design variables and applications, Biomaterials 24 (24) (2003) 4337–4351.
[10] I.L. Kim, R.L. Mauck, J.A. Burdick, Hydrogel design for cartilage tissue engineering: a case study with hyaluronic acid, Biomaterials 32 (34) (2011) 8771–8782.
[11] O. Jeon, C. Powell, S.M. Ahmed, E. Alsberg, Biodegradable, photocrosslinked alginate hydrogels with independently tailorable physical properties and cell adhesivity, Tissue Eng. Part A 16 (9) (2010) 2915–2925.
[12] J. Wang, F. Zhang, W.P. Tsang, C. Wan, C. Wu, Fabrication of injectable high strength hydrogel based on 4-arm star PEG for cartilage tissue engineering, Biomaterials 120 (2017) 11–21.
[13] A. Naumann, J.E. Dennis, J. Aigner, J. Coticchia, J. Arnold, A. Berghaus, E.R. Kastenbauer, A.I. Caplan, Tissue engineering of autologous cartilage grafts in three-dimensional *in vitro* macroaggregate culture system, Tissue Eng. 10 (11–12) (2004) 1695–1706.
[14] T. Mesallati, C.T. Buckley, D.J. Kelly, Engineering articular cartilage-like grafts by self-assembly of infrapatellar fat pad-derived stem cells, Biotechnol. Bioeng. 111 (8) (2014) 1686–1698.
[15] J.C. Hu, K.A. Athanasiou, A self-assembling process in articular cartilage tissue engineering, Tissue Eng. 12 (4) (2006) 969–979.
[16] J.J. Ng, Y. Wei, B. Zhou, J. Bernhard, S. Robinson, A. Burapachaisri, X.E. Guo, G. Vunjak-Novakovic, Recapitulation of physiological spatiotemporal signals promotes *in vitro* formation of phenotypically stable human articular cartilage, Proc. Natl. Acad. Sci. U.S.A. 114 (10) (2017) 2556–2561.
[17] K.A. Athanasiou, R. Eswaramoorthy, P. Hadidi, J.C. Hu, Self-organization and the self-assembling process in tissue engineering, Annu .Rev. Biomed. Eng. 15 (2013) 115–136.
[18] J.H. Shim, K.M. Jang, S.K. Hahn, J.Y. Park, H. Jung, K. Oh, K.M. Park, J. Yeom, S.H. Park, S.W. Kim, J.H. Wang, K. Kim, D.W. Cho, Three-dimensional bioprinting of multilayered constructs containing human mesenchymal stromal cells for osteochondral tissue regeneration in the rabbit knee joint, Biofabrication 8 (1) (2016) 014102.
[19] T. Mesallati, E.J. Sheehy, T. Vinardell, C.T. Buckley, D.J. Kelly, Tissue engineering scaled-up, anatomically shaped osteochondral constructs for joint resurfacing, Eur. Cell Mater. 30 (2015) 163–185 discussion 185-6.
[20] E. Farrell, O.P. Van Der Jagt, W. Koevoet, N. Kops, C.J. Van Manen, C.A. Hellingman, H. Jahr, F.J. O'Brien, J.A.N. Verhaar, H. Weinans, G.J.V.M. Van Osch, Chondrogenic priming of human bone marrow stromal cells: a better route to bone repair? Tissue Eng. Part C Methods 15 (2) (2009) 285–295.
[21] D. Gawlitta, E. Farrell, J. Malda, L.B. Creemers, J. Alblas, W.J.A. Dhert, Modulating endochondral ossification of multipotent stromal cells for bone regeneration, Tissue Eng. Part B: Rev. 16 (4) (2010) 385–395.
[22] C. Scotti, B. Tonnarelli, A. Papadimitropoulos, A. Scherberich, S. Schaeren, A. Schauerte, J. Lopez-Rios, R. Zeller, A. Barbero, I. Martin, Recapitulation of endochondral bone formation using human adult mesenchymal stem cells as a paradigm for developmental engineering, Proc. Natl. Acad. Sci. U.S.A. 107 (16) (2010) 7251–7256.
[23] S. Critchley, G. Cunniffe, A. O'Reilly, P. Diaz-Payno, R. Schipani, A. McAlinden, D. Withers, J. Shin, E. Alsberg, D.J. Kelly, Regeneration of Osteochondral Defects Using Developmentally Inspired Cartilaginous Templates, Tissue Eng. Part A 25 (3–4) (2019) 159–171.
[24] E.J. Sheehy, D.J. Kelly, F.J. O'Brien, Biomaterial-based endochondral bone regeneration: a shift from traditional tissue engineering paradigms to developmentally inspired strategies, Mater. Today Bio. 3 (2019) 100009.
[25] E.B. Hunziker, E. Kapfinger, J. Geiss, The structural architecture of adult mammalian articular cartilage evolves by a synchronized process of tissue resorption and neoformation during postnatal development, Osteoarthritis Cartil. 15 (4) (2007) 403–413.
[26] K.M. Hubka, R.L. Dahlin, V.V. Meretoja, F.K. Kasper, A.G. Mikos, Enhancing chondrogenic phenotype for cartilage tissue engineering: monoculture and co-culture of articular chondrocytes and mesenchymal stem cells, Tissue Eng. Part B Rev. 20 (6) (2014) 641–654.
[27] V.V. Meretoja, R.L. Dahlin, F.K. Kasper, A.G. Mikos, Enhanced chondrogenesis in co-cultures with articular chondrocytes and mesenchymal stem cells, Biomaterials 33 (27) (2012) 6362–6369.
[28] L. Bian, D.Y. Zhai, R.L. Mauck, J.A. Burdick, Coculture of human mesenchymal stem cells and articular chondrocytes reduces hypertrophy and enhances functional properties of engineered cartilage, Tissue Eng. Part A 17 (7–8) (2011) 1137–1145.

[29] S.J. Bryant, K.S. Anseth, Hydrogel properties influence ECM production by chondrocytes photoencapsulated in poly(ethylene glycol) hydrogels, J. Biomed. Mater. Res. 59 (1) (2002) 63–72.
[30] F.E. Freeman, D.J. Kelly, Tuning alginate bioink stiffness and composition for controlled growth factor delivery and to spatially direct MSC fate within bioprinted tissues, Sci. Rep. 7 (1) (2017) 17042.
[31] C.M. Homenick, G. de Silveira, H. Sheardown, A. Adronov, Pluronics as crosslinking agents for collagen: novel amphiphilic hydrogels, Polym. Int. 60 (3) (2011) 458–465.
[32] H. Duong, B. Wu, B. Tawil, Modulation of 3D fibrin matrix stiffness by intrinsic fibrinogen-thrombin compositions and by extrinsic cellular activity, Tissue Eng. Part A 15 (7) (2009) 1865–1876.
[33] C.R. Lee, A.J. Grodzinsky, M. Spector, The effects of cross-linking of collagen-glycosaminoglycan scaffolds on compressive stiffness, chondrocyte-mediated contraction, proliferation and biosynthesis, Biomaterials 22 (23) (2001) 3145–3154.
[34] G.C. Ingavle, A.W. Frei, S.H. Gehrke, M.S. Detamore, Incorporation of aggrecan in interpenetrating network hydrogels to improve cellular performance for cartilage tissue engineering, Tissue Eng. Part A 19 (11–12) (2013) 1349–1359.
[35] S. Rossana, S. Stefan, F. Romain, E.C. Susan, K. Daniel John, Reinforcing interpenetrating network hydrogels with 3D printed polymer networks to engineer cartilage mimetic composites, Biofabrication (2020).
[36] B. Deorosan, E.A. Nauman, The role of glucose, serum, and three-dimensional cell culture on the metabolism of bone marrow-derived mesenchymal stem cells, Stem Cells Int. 2011 (2011) 429187.
[37] W. Bensaid, J.T. Triffitt, C. Blanchat, K. Oudina, L. Sedel, H. Petite, A biodegradable fibrin scaffold for mesenchymal stem cell transplantation, Biomaterials 24 (14) (2003) 2497–2502.
[38] Y. Wu, S. Joseph, N.R. Aluru, Effect of cross-linking on the diffusion of water, ions, and small molecules in hydrogels, J. Phys. Chem. B 113 (11) (2009) 3512–3520.
[39] I.E. Erickson, A.H. Huang, S. Sengupta, S. Kestle, J.A. Burdick, R.L. Mauck, Macromer density influences mesenchymal stem cell chondrogenesis and maturation in photocrosslinked hyaluronic acid hydrogels, Osteoarthritis Cartilage 17 (12) (2009) 1639–1648.
[40] B.V. Sridhar, J.L. Brock, J.S. Silver, J.L. Leight, M.A. Randolph, K.S. Anseth, Development of a cellularly degradable PEG hydrogel to promote articular cartilage extracellular matrix deposition, Adv. Healthc. Mater. 4 (5) (2015) 702–713.
[41] A.J. Engler, S. Sen, H.L. Sweeney, D.E. Discher, Matrix elasticity directs stem cell lineage specification, Cell 126 (4) (2006) 677–689.
[42] O. Chaudhuri, L. Gu, D. Klumpers, M. Darnell, S.A. Bencherif, J.C. Weaver, N. Huebsch, H.-p. Lee, E. Lippens, G.N. Duda, D.J. Mooney, Hydrogels with tunable stress relaxation regulate stem cell fate and activity, Nat. Mater. 15 (3) (2016) 326–334.
[43] C.A. DeForest, K.S. Anseth, Advances in bioactive hydrogels to probe and direct cell fate, Annu. Rev. Chem. Biomol. Eng. 3 (2012) 421–444.
[44] J. Malda, J. Visser, F.P. Melchels, T. Jüngst, W.E. Hennink, W.J.A. Dhert, J. Groll, D.W. Hutmacher, 25th Anniversary Article: engineering Hydrogels for Biofabrication, Adv. Mater. 25 (36) (2013) 5011–5028.
[45] J. Kundu, J.H. Shim, J. Jang, S.W. Kim, D.W. Cho, An additive manufacturing-based PCL-alginate-chondrocyte bioprinted scaffold for cartilage tissue engineering, J. Tissue Eng. Regen. Med. 9 (11) (2015) 1286–1297.
[46] A.C. Daly, G.M. Cunniffe, B.N. Sathy, O. Jeon, E. Alsberg, D.J. Kelly, 3D bioprinting of developmentally inspired templates for whole bone organ engineering, Adv. Healthc. Mater. 5 (18) (2016) 2353–2362.
[47] H.W. Kang, S.J. Lee, I.K. Ko, C. Kengla, J.J. Yoo, A. Atala, A 3D bioprinting system to produce human-scale tissue constructs with structural integrity, Nat. Biotechnol. 34 (3) (2016) 312–319.
[48] J. Visser, F.P.W. Melchels, J.E. Jeon, E.M. van Bussel, L.S. Kimpton, H.M. Byrne, W.J.A. Dhert, P.D. Dalton, D.W. Hutmacher, J. Malda, Reinforcement of hydrogels using three-dimensionally printed microfibres, Nat. Commun. 6 (1) (2015) 6933.
[49] J.C. Middleton, A.J. Tipton, Synthetic biodegradable polymers as orthopedic devices, Biomaterials 21 (23) (2000) 2335–2346.
[50] M.A. Woodruff, D.W. Hutmacher, The return of a forgotten polymer—Polycaprolactone in the 21st century, Prog. Polym. Sci. 35 (10) (2010) 1217–1256.
[51] A.D. Olubamiji, Z. Izadifar, J.L. Si, D.M. Cooper, B.F. Eames, D.X. Chen, Modulating mechanical behaviour of 3D-printed cartilage-mimetic PCL scaffolds: influence of molecular weight and pore geometry, Biofabrication 8 (2) (2016) 025020.
[52] R. Schipani, D.R. Nolan, C. Lally, D.J. Kelly, Integrating finite element modelling and 3D printing to engineer biomimetic polymeric scaffolds for tissue engineering, Connect. Tissue Res. 61 (2) (2020) 174–189.
[53] H. Sun, L. Mei, C. Song, X. Cui, P. Wang, The *in vivo* degradation, absorption and excretion of PCL-based implant, Biomaterials 27 (9) (2006) 1735–1740.
[54] Z. Pan, J. Ding, Poly(lactide-co-glycolide) porous scaffolds for tissue engineering and regenerative medicine, Interface Focus 2 (3) (2012) 366–377.
[55] L.S. Nair, C.T. Laurencin, Biodegradable polymers as biomaterials, Prog. Polym. Sci. 32 (8) (2007) 762–798.
[56] C. Shasteen, Y.B. Choy, Controlling degradation rate of poly(lactic acid) for its biomedical applications, Biomed. Eng. Lett. 1 (3) (2011) 163.
[57] C.H. Lee, S.A. Rodeo, L.A. Fortier, C. Lu, C. Erisken, J.J. Mao, Protein-releasing polymeric scaffolds induce fibrochondrocytic differentiation of endogenous cells for knee meniscus regeneration in sheep, Sci. Transl. Med. 6 (266) (2014) 266ra171.
[58] W. Wang, B. Li, J. Yang, L. Xin, Y. Li, H. Yin, Y. Qi, Y. Jiang, H. Ouyang, C. Gao, The restoration of full-thickness cartilage defects with BMSCs and TGF–beta 1 loaded PLGA/fibrin gel constructs, Biomaterials 31 (34) (2010) 8964–8973.
[59] T. Hickey, D. Kreutzer, D.J. Burgess, F. Moussy, Dexamethasone/PLGA microspheres for continuous delivery of an anti-inflammatory drug for implantable medical devices, Biomaterials 23 (7) (2002) 1649–1656.
[60] T. Guo, T.R. Holzberg, C.G. Lim, F. Gao, A. Gargava, J.E. Trachtenberg, A.G. Mikos, J.P. Fisher, 3D printing PLGA: a quantitative examination of the effects of polymer composition and printing parameters on print resolution, Biofabrication 9 (2) (2017) 024101.
[61] E. Dawson, G. Mapili, K. Erickson, S. Taqvi, K. Roy, Biomaterials for stem cell differentiation, Adv. Drug Deliv. Rev. 60 (2) (2008) 215–228.
[62] A. van Sliedregt, M. Knook, S.C. Hesseling, H.K. Koerten, K. de Groot, C.A. van Blitterswijk, Cellular reaction on the intraperitoneal injection of four types of polylactide particulates, Biomaterials 13 (12) (1992) 819–824.
[63] M.S. Kim, H.H. Ahn, Y.N. Shin, M.H. Cho, G. Khang, H.B. Lee, An *in vivo* study of the host tissue response to subcutaneous implantation of PLGA-and/or porcine small intestinal submucosa-based scaffolds, Biomaterials 28 (34) (2007) 5137–5143.
[64] KH Bouhadir , KY Lee, E Alsberg, KW Damm, DJ Mooney, Degradation of Partially Oxidized Alginate and Its Potential Application for Tissue Engineering, Biotechnol Prog. 17 (5) (2000) 945–950, doi:10.1021/bp010070p.
[65] T. Vinardell, E.J. Sheehy, C.T. Buckley, D.J. Kelly, A comparison of the functionality and *in vivo* phenotypic stability of cartilaginous tissues engineered from different stem cell sources, Tissue Eng. Part A 18 (11–12) (2012) 1161–1170.
[66] D. Olvera, A. Daly, D.J. Kelly, Mechanical testing of cartilage constructs, Methods Mol. Biol. 1340 (2015) 279–287.
[67] T.J. Levingstone, A. Ramesh, R.T. Brady, P.A.J. Brama, C. Kearney, J.P. Gleeson, F.J. O'Brien, Cell-free multi-layered collagen-based scaffolds demonstrate layer specific regeneration of functional osteochondral tissue in caprine joints, Biomaterials 87 (2016) 69–81.
[68] G.M. Cunniffe, P.J. Diaz-Payno, E.J. Sheehy, S.E. Critchley, H.V. Almeida, P. Pitacco, S.F. Carroll, O.R. Mahon, A. Dunne, T.J. Levingstone, C.J. Moran, R.T. Brady, F.J. O'Brien, P.A.J. Brama, D.J. Kelly, Tissue-specific extracellular matrix scaffolds for the regeneration of spatially complex musculoskeletal tissues, Biomaterials 188 (2019) 63–73.
[69] N. Reznikov, R. Almany-Magal, R. Shahar, S. Weiner, Three-dimensional imaging of collagen fibril organization in rat circumferential lamellar bone using a dual beam electron microscope reveals ordered and disordered sub-lamellar structures, Bone 52 (2) (2013) 676–683.
[70] S.H. Elder, A.J. Cooley Jr., A. Borazjani, B.L. Sowell, H. To, S.C. Tran, Production of hyaline-like cartilage by bone marrow mesenchymal stem cells in a self--assembly model, Tissue Eng. Part A 15 (10) (2009) 3025–3036.
[71] C.E. Holy, C. Cheng, J.E. Davies, M.S. Shoichet, Optimizing the sterilization of PLGA scaffolds for use in tissue engineering, Biomaterials 22 (1) (2001) 25–31.
[72] H. Shearer, M.J. Ellis, S.P. Perera, J.B. Chaudhuri, Effects of common sterilization methods on the structure and properties of poly(D,L lactic-co-glycolic acid) scaffolds, Tissue Eng. 12 (10) (2006) 2717–2727.
[73] H. Fan, Y. Hu, C. Zhang, X. Li, R. Lv, L. Qin, R. Zhu, Cartilage regeneration using mesenchymal stem cells and a PLGA-gelatin/chondroitin/hyaluronate hybrid scaffold, Biomaterials 27 (26) (2006) 4573–4580.
[74] T. Tanaka, M. Hirose, N. Kotobuki, M. Tadokoro, H. Ohgushi, T. Fukuchi, J. Sato, K. Seto, Bone augmentation by bone marrow mesenchymal stem cells cultured in three-dimensional biodegradable polymer scaffolds, J. Biomed. Mater. Res. A 91 (2) (2009) 428–435.
[75] X. Xin, M. Hussain, J.J. Mao, Continuing differentiation of human mesenchymal stem cells and induced chondrogenic and osteogenic lineages in electrospun PLGA nanofiber scaffold, Biomaterials 28 (2) (2007) 316–325.
[76] J.Y. Kim, D.-.W. Cho, Blended PCL/PLGA scaffold fabrication using multi-head deposition system, Microelectron Eng. 86 (4) (2009) 1447–1450.
[77] L. Lu, S.J. Peter, M.D. Lyman, H.L. Lai, S.M. Leite, J.A. Tamada, S. Uyama, J.P. Vacanti, R. Langer, A.G. Mikos, *In vitro* and *in vivo* degradation of porous poly(DL-lactic-co-glycolic acid) foams, Biomaterials 21 (18) (2000) 1837–1845.
[78] J.H. Shim, T.S. Moon, M.J. Yun, Y.C. Jeon, C.M. Jeong, D.W. Cho, J.B. Huh, Stimulation of healing within a rabbit calvarial defect by a PCL/PLGA scaffold blended with TCP using solid freeform fabrication technology, J. Mater. Sci. Mater. Med. 23 (12) (2012) 2993–3002.
[79] A.C. Vieira, J.C. Vieira, J.M. Ferra, F.D. Magalhaes, R.M. Guedes, A.T. Marques, Mechanical study of PLA-PCL fibers during *in vitro* degradation, J. Mech. Behav. Biomed. Mater. 4 (3) (2011) 451–460.
[80] N.T. Hiep, B.T. Lee, Electro-spinning of PLGA/PCL blends for tissue engineering and their biocompatibility, J. Mater. Sci. Mater. Med. 21 (6) (2010) 1969–1978.
[81] T. Schinkothe, W. Bloch, A. Schmidt, *In vitro* secreting profile of human mesenchymal stem cells, Stem Cells Dev. 17 (1) (2008) 199–206.
[82] G.M. van Buul, E. Villafuertes, P.K. Bos, J.H. Waarsing, N. Kops, R. Narcisi, H. Weinans, J.A. Verhaar, M.R. Bernsen, G.J. van Osch, Mesenchymal stem cells secrete factors that inhibit inflammatory processes in short-term osteoarthritic synovium and cartilage explant culture, Osteoarthritis Cartilage 20 (10) (2012) 1186–1196.
[83] W.H. Chen, M.T. Lai, A.T. Wu, C.C. Wu, J.G. Gelovani, C.T. Lin, S.C. Hung, W.T. Chiu, W.P. Deng, *In vitro* stage-specific chondrogenesis of mesenchymal stem cells committed to chondrocytes, Arthritis Rheum. 60 (2) (2009) 450–459.

[84] L. Wu, J.C.H. Leijten, N. Georgi, J.N. Post, C.A. Van Blitterswijk, M. Karperien, Trophic effects of mesenchymal stem cells increase chondrocyte proliferation and matrix formation, Tissue Eng. Part A 17 (9–10) (2011) 1425–1436.
[85] C. Acharya, A. Adesida, P. Zajac, M. Mumme, J. Riesle, I. Martin, A. Barbero, Enhanced chondrocyte proliferation and mesenchymal stromal cells chondrogenesis in coculture pellets mediate improved cartilage formation, J. Cell Physiol. 227 (1) (2012) 88–97.
[86] T.S. de Windt, J.A. Hendriks, X. Zhao, L.A. Vonk, L.B. Creemers, W.J. Dhert, M.A. Randolph, D.B. Saris, Concise review: unraveling stem cell cocultures in regenerative medicine: which cell interactions steer cartilage regeneration and how? Stem Cells Transl. Med. 3 (6) (2014) 723–733.
[87] J. Diaz-Romero, J.P. Gaillard, S.P. Grogan, D. Nesic, T. Trub, P. Mainil-Varlet, Immunophenotypic analysis of human articular chondrocytes: changes in surface markers associated with cell expansion in monolayer culture, J. Cell Physiol. 202 (3) (2005) 731–742.
[88] E. Kon, M. Delcogliano, G. Filardo, M. Fini, G. Giavaresi, S. Francioli, I. Martin, D. Pressato, E. Arcangeli, R. Quarto, M. Sandri, M. Marcacci, Orderly osteochondral regeneration in a sheep model using a novel nano-composite multilayered biomaterial, J. Orthopaed. Res. 28 (1) (2010) 116–124 official publication of the Orthopaedic Research Society.
[89] A.R. Gannon, T. Nagel, A.P. Bell, N.C. Avery, D.J. Kelly, Postnatal changes to the mechanical properties of articular cartilage are driven by the evolution of its collagen network, Eur. Cell Mater. 29 (2015) 105–121 discussion 121-3.
[90] E. Varoni, M. Tschon, B. Palazzo, P. Nitti, L. Martini, L. Rimondini, Agarose gel as biomaterial or scaffold for implantation surgery: characterization, histological and histomorphometric study on soft tissue response, Connect Tissue Res. 53 (6) (2012) 548–554.
[91] T.M. Robinson, D.W. Hutmacher, P.D. Dalton, The Next Frontier in Melt Electrospinning: taming the Jet, Adv. Funct. Mater. 29 (44) (2019) 1904664.
[92] E.J. Sheehy, T. Vinardell, M.E. Toner, C.T. Buckley, D.J. Kelly, Altering the architecture of tissue engineered hypertrophic cartilaginous grafts facilitates vascularisation and accelerates mineralisation, PLoS ONE 9 (3) (2014).
[93] M.J.F. Blumer, S. Longato, H. Fritsch, Structure, formation and role of cartilage canals in the developing bone, Ann. Anatomy 190 (4) (2008) 305–315.
[94] M. Kesti, C. Eberhardt, G. Pagliccia, D. Kenkel, D. Grande, A. Boss, M. Zenobi–Wong, Bioprinting: bioprinting complex cartilaginous structures with clinically compliant biomaterials, Adv. Funct. Mater. 25 (48) (2015) 7397–7397.
[95] J. Visser, B. Peters, T.J. Burger, J. Boomstra, W.J. Dhert, F.P. Melchels, J. Malda, Biofabrication of multi-material anatomically shaped tissue constructs, Biofabrication 5 (3) (2013) 035007.
[96] Y. Jin, A. Compaan, T. Bhattacharjee, Y. Huang, Granular gel support-enabled extrusion of three-dimensional alginate and cellular structures, Biofabrication 8 (2) (2016) 025016.
[97] A.C. Daly, P. Pitacco, J. Nulty, G.M. Cunniffe, D.J. Kelly, 3D printed microchannel networks to direct vascularisation during endochondral bone repair, Biomaterials 162 (2018) 34–46.
[98] E.S. Place, N.D. Evans, M.M. Stevens, Complexity in biomaterials for tissue engineering, Nat. Mater. 8 (6) (2009) 457–470.
[99] M.M. Stevens, R.P. Marini, D. Schaefer, J. Aronson, R. Langer, V.P. Shastri, *In vivo* engineering of organs: the bone bioreactor, Proc. Natl. Acad. Sci. U.S.A. 102 (32) (2005) 11450–11455.